JGR Atmospheres

RESEARCH ARTICLE
10.1029/2023JD038694

Investigating the Effect of Aerosol Uncertainty on Convective Precipitation Forecasting in South China's Coastal Area

Yueya Wang[1], Zijing Zhang[1], Wing Sze Chow[2], Zhe Wang[1], Jian Zhen Yu[1,2], Jimmy Chi-Hung Fung[1,3], and Xiaoming Shi[1]

[1]Division of Environment and Sustainability, Hong Kong University of Science and Technology, Hong Kong, China, [2]Department of Chemistry, Hong Kong University of Science and Technology, Hong Kong, China, [3]Department of Mathematics, Hong Kong University of Science and Technology, Hong Kong, China

Key Points:

- Deceasing water-friendly (WF) aerosol generates more precipitation, and increasing ice-friendly (IF) aerosol enhances precipitation intensity
- Deceasing WF aerosol triggers early convection initiation while increasing IF aerosol results in stronger initiation
- Nonlinear relationship exists between the aerosol concentration and convection intensity

Correspondence to:
X. Shi,
shixm@ust.hk

Citation:
Wang, Y., Zhang, Z., Chow, W. S., Wang, Z., Yu, J. Z., Fung, J. C.-H, & Shi, X. (2023). Investigating the effect of aerosol uncertainty on convective precipitation forecasting in South China's coastal area. *Journal of Geophysical Research: Atmospheres*, *128*, e2023JD038694. https://doi.org/10.1029/2023JD038694

Received 13 MAR 2023
Accepted 14 MAY 2023

Abstract Previous studies on convective precipitation forecasting in South China have focused on the effects of multiscale dynamics and microphysics parameterizations. However, limited investigation has been conducted on how uncertainty in aerosol data might cause errors in quantitative precipitation forecast for South China's coastal convection. In this case study, we evaluated the impact of aerosol uncertainties on South China's severe coastal convection using convection-permitting simulations. We estimated the variability range of aerosol concentrations with observations for the pre-summer months. The simulation results suggest that the rainfall pattern and intensity change notably when aerosol concentrations are varied. Decreasing the concentration of water-friendly (WF) aerosols intensifies precipitation through reduced cloud water number concentration and increased droplet size. Increasing the concentration of ice-friendly (IF) aerosols results in up to 40% increase in vertical velocity and latent heat compared to minimal IF aerosol condition, by enhancing the heterogeneous process and dynamically intensifying convection. Consequently, the simulation with minimal WF and maximal IF aerosol concentrations shows prolonged intense precipitation over the entire life cycle of convection. However, when both WF and IF aerosols are set to minimal concentrations, the simulation produces the maximum peak rainfall rate, which is about 50% stronger than the simulation with the climatological mean concentration, due to an enhanced homogeneous process that results in a higher ice concentration and more efficient ice-phase precipitation growth. Meanwhile, variation in aerosol concentration affects convection initiation (CI), with a lower concentration of WF aerosol inducing earlier CI onset. Decreasing hygroscopicity leads to higher precipitation.

Plain Language Summary Convective weather frequently happens in South China during the pre-summer season with limited forecast skills. Previous studies have investigated the impact of large-scale circulation, water vapor conditions, and complex topography in forming convective precipitation systems. However, how chemistry interacts with weather dynamics has limited investigation in the context of convective weather in South China's coastal area. Aerosols can serve as cloud condensation nuclei (CCN) and ice nuclei (IN), and their concentration or property variation can affect various processes in cloud and precipitation formation. To estimate the impact of aerosol uncertainty on South China's pre-summer rainfall, we conducted simulations of a severe convection case with different aerosol concentrations and properties. We found that the typical aerosol concentration and property variability changed the convective system notably, which further influenced the rainfall pattern and intensity. The aerosols invigorate convection when they cause more latent heating or shift the vertical heating distribution upward, for instance, decreasing the water-friendly aerosol or increasing the ice-friendly aerosol can enhance the convection. This work contributes to understanding the aerosol effects of different kinds of aerosols on convection initiation, and precipitation intensity and suggests the potential benefits of increasing aerosol observations in the future to improve the operational numerical forecast.

1. Introduction

Intense convection frequently occurs during the April to June (pre-summer) rainy season in South China and produces almost half the amount of local annual rainfall. Severe flooding resulting from extreme precipitation in this season often endangers the safety of lives and causes substantial economic losses (Luo et al., 2017). Previous studies examined the occurrence and properties of the pre-summer heavy rainfall in South China from the perspectives of large-scale circulation, synoptic pattern, mesoscale processes (such as interactions between

convectively generated shallow cold-pool and moist, unstable boundary air with tropical origin), storm-scale dynamics, and cloud-precipitation microphysics (e.g., Bao et al., 2021; G. Chen et al., 2018; M. Li et al., 2022; Z. Li et al., 2020; Luo et al., 2017; Wang et al., 2014; Yu et al., 2023). It is found that a large fraction of the pre-summer rainfall is produced by convection in the warm sector region hundreds of kilometers ahead of a cold or quasi-stationary front. However, the convection initiation (CI), which depends on the multiscale interaction of atmospheric dynamics, is known for its notoriously low predictability in the warm sector regions (Bai et al., 2021; Luo et al., 2017; Zhang et al., 2022). Therefore, the warm-sector CI and the following convection development are major contributors to the errors in quantitative precipitation forecast (QPF) for the region. Recent studies revealed that a few factors, including low-level jets, small-scale variability of moisture pooling, and local orography together regulate the CI, rendering its accurate prediction very challenging (Bai et al., 2021; Du & Chen, 2018, 2019b). The magnitude of land-sea thermal contrast and city agglomeration over coastal South China also play important roles in regulating the initiation and development of coastal convection (Gao et al., 2022; Sun et al., 2021; Wu et al., 2019).

Besides the complexity of dynamics, uncertainties in microphysics parameterizations can also strongly affect the prediction of the convective rainfall in the South China region. Qian et al. (2018) found that although using different microphysics schemes did not strongly affect CI, the movement and organization of simulated squall lines are sensitive to the variation of microphysics parameterizations. Yin et al. (2018) suggest that latent heating is an important factor in governing the intensity of convection, while rain evaporation is also suggested as a critical process due to its effect on regulating cold pool intensity (Qian et al., 2018; Zhao et al., 2021; Zhou et al., 2022). Zhao et al. (2021) further highlighted the impact of the accurate and flexible representation of ice particle properties on simulating the transition zone between the convective and stratiform precipitation regions in a squall line.

The atmospheric chemistry, namely aerosols, plays a role in affecting the QPF in South China's coastal area through interactions with cloud microphysics. A recent study based on radar and distrometer observations on the extreme precipitation for South China suggests that raindrops in this region have sizes larger than the typical "maritime" regime but number concentrations higher than the typical "continental" regime (Yu et al., 2022). Such unique characteristics of hydrometers may reflect the complexity of the aerosol source and composition in this region due to its coastal location and the development of industries in South China (Wong et al., 2022). Aerosols play the roles of cloud condensation nuclei (CCN) and ice nuclei (IN), and therefore the variability of aerosol composition and concentration can directly change cloud characteristics and indirectly influence the radiation budget of the atmosphere, the accuracy of which is critical for successful climate modeling. Idealized numerical simulations have helped to make important progress on the interaction between aerosols and convective systems. However, it is still unclear how relevant the uncertainties in aerosol information are to the QPF in a particular region. This issue is partially a result of the complexity of aerosol-dynamics interaction depending on detailed characteristics of deep convection over different regions (Fan et al., 2016). The other factor is the idealized approach adopted by some previous studies, which often compare arbitrarily defined "pristine" and "polluted" conditions with the concentration of aerosols differing from a factor of ten to a few orders of magnitude (e.g., Chang et al., 2021; Q. Chen et al., 2019; Furtado et al., 2018; Guo et al., 2022; Miyamoto, 2021). Furtado et al. (2020) investigated the surface rainfall change with spanned range of extremely clean to extremely polluted conditions to demonstrate the aerosol effect. Researchers had to design their experiments in such an idealized way because of the lack of long-term concurrent observation of aerosol properties that can address the covariability of aerosols, dynamics, and thermodynamics (Fan et al., 2016).

In this study, we use available observations of aerosols properties in Hong Kong to estimate the range of their variability and employ the Weather Research and Forecasting (WRF) model with the aerosol-aware Thompson microphysics scheme (Thompson & Eidhammer, 2014) to semi-quantitatively assess the impact of the uncertainties of aerosol information on the QPF of South China coastal region convection. We examined the impact on the CI of different aerosol concentrations. Variations in convection intensity and the related dynamics and thermodynamics environments are discussed to understand the aerosol effect further. In addition, two simulations with hygroscopicity value suggested by the observation are conducted to evaluate the influence of hygroscopicity.

2. Methods and Experiments

2.1. Case Description

We conducted our experiments with the severe convective rainstorm case on 27–28 June 2021, in Hong Kong. It is categorized as a "black rainstorm" (hourly rainfall exceeding 70 mm) according to Hong Kong Observatory's

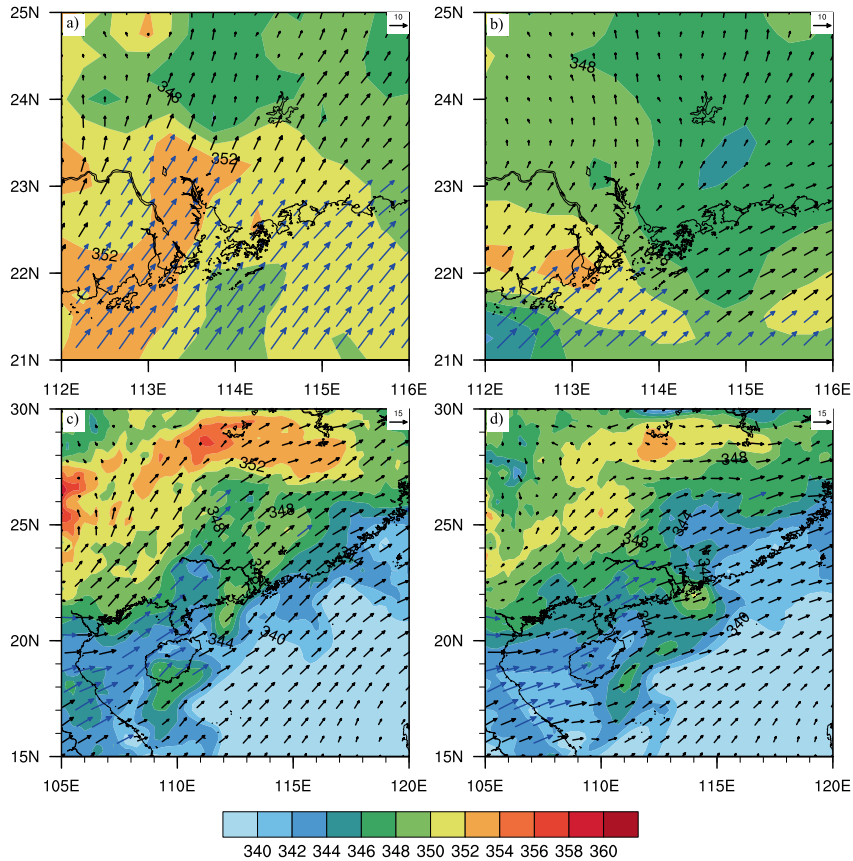

Figure 1. The wind (arrows) and equivalent potential temperature (shading) (K) at 1800 UTC, 27 (left column) and 0000 UTC, 28 (right column) June at different pressure levels: (a), (b) 950 hPa, (c), (d) 850 hPa. Southernly winds with wind speed over 10 m/s in (a), (b) and 15 m/s in (c), (d) are indicated by blue arrows in panels. The black lines indicate the coastline.

(HKO) rainstorm warning system. The heavy rainfall occurs at the forefront of the marine boundary layer jet as shown in Figure 1 with wind larger than 10 m/s at 950 hPa and 15 m/s at 850 hPa along the coast of the South China Sea, which is often associated with warm sector convection (Du & Chen, 2019a). This case is not typical in that the cold front to the west of Hong Kong is weak, if not absent. Nevertheless, the active southwesterly airstream does bring warm moist flow with high equivalent potential temperature (Figures 1c and 1d) from the South China Sea to the coast of Guangdong. The precipitation was intense and persistent on the morning of 28 June, and a black rainstorm warning was issued. Over 150 mm daily rainfall were recorded at many observation stations (Figure 4f). The numerical forecast with a resolution of 2 km underestimated the precipitation and led to a late issuing of the black rainstorm warning on the morning of 28 June (HKO, 2021).

2.2. Experiment Design

The simulation was configured with three nested domains with horizontal grid resolutions of 9, 3, and 1 km, respectively, using the WRF model version 4.3.1. The vertical direction has 51 levels up to the model top at 50 hPa. Each simulation was run for 24 hr, starting from 06 UTC on 27 June 2021. The Thompson aerosol-aware microphysics scheme was employed in the simulations. The aerosols in the scheme are divided into water-friendly (WF) aerosols for CCN and ice-friendly (IF) aerosols for IN. The initial and boundary condition for the Thompson aerosol aware scheme are from the scaled two kinds of aerosols. The aerosols are then advected and diffused during the simulation. In addition, a variable lower boundary condition based on the starting near-surface aerosol concentration is implemented with a mean surface wind to calculate the surface emission flux at the lowest model level (Thompson & Eidhammer, 2014). The CCN activation is based on a look-up table which is derived from the Köhler activation theory with a parcel model, and the IN-number concentration follows the parameterization of DeMott et al. (2010). The WF aerosol is comprised of sulfates, nitrate, sea salts, and organic carbon (OC), and

Table 1
Weather Research and Forecasting Configuration for the Simulations

Parameterization	Scheme
Initial and boundary condition	ECMWF Reanalysis V5 (ERA5)
Microphysics	Thompson aerosol-aware
Long-wave radiation	RRTM
Short-wave radiation	RRTM
Surface	Noah Land Surface Model
PBL	ACM2

the IF aerosol is primarily considered to be dust. The aerosol emissions are simplified and represented based on the starting near-surface aerosol concentrations. The scheme is a bulk microphysics scheme and has double moment ice and rain. Other model configuration details are shown in Table 1.

A set of simulations were run to test the impact of different aerosol states with varying WF and IF aerosol concentrations on the cloud and precipitation development. The default option for the aerosol-aware scheme is to use the climatological mean aerosol concentration derived from the 7 years (2001–2007) simulation of the Goddard Chemistry Aerosol Radiation and Transport (GOCART) model (Colarco et al., 2010; Thompson & Eidhammer, 2014). Our simulation using this default option is denoted as the "Climatology" experiment as a reference.

For sensitivity tests, we adjust the aerosol concentration based on the observed variability of aerosols in Hong Kong. Observational aerosol data are available for April to June 2020 at the Tuen Mun Air Quality Monitoring Station in Hong Kong (22°23′28.4″N, 113°58′37.1″E, 30 m above ground level) (Wong et al., 2022). Since the observatory data is near the surface, the scale factor is calculated with respect to the lowest level of the GOCART climatology data. The mass concentration of chemical species, including SO_4^{2-}, NO_3^-, Na^+, OC and Al were obtained every 3 days. The number concentration of the WF aerosol (including sulfates, nitrate, sea salts, and OC) and IF aerosol (i.e., dust) was calculated from the observation of related ion mass concentration by assuming that the aerosol size distribution follows a lognormal distribution. The characteristic diameter and geometric standard deviation from the analysis results of Bian et al. (2014) were used, and we assumed the aerosols were externally mixed. The 3-month time series of the number concentration of those aerosols in the observation period are shown in Figure 2. In that period, the maximum values of the WF and IF aerosol number concentrations are 0.818 and 0.795 times, respectively, of the GOCART climatological monthly mean value for the precipitation event; the minima are 0.045 and 0.080 times, respectively, of the GOCART value. We scale the aerosol data for entire simulation domains with those factors to roughly represent the range of aerosol concentration variability in the pre-summer season. In reality, different levels may vary by different amounts in different days. We scaled the entire profile by the same scaling factor determined by surface observation due to lack of free atmosphere aerosol observations. It is not uncommon to vary aerosol concentrations in such a way and has been used in previous studies (e.g., Thompson & Eidhammer, 2014). By combing the maximum and the minimum of the aerosol number concentrations, we obtain four different experiments denoted as "WmaxImax," "WmaxImin," "WminImax," and "WminImin," where "W" and "I" indicate WF and IF aerosols, respectively, and "max" or "min" following "W" or "I" indicates the scaling factor corresponding to the maximum or minimum bounds of the associated aerosol group. To further understand the effect of aerosols on precipitation, we conducted two additional experiments referred to as "WmedImed" and "WmorImor." In the WmedImed simulation, aerosol concentrations were adjusted to the median value of the observation. In the WmorImor simulation, aerosol concentrations were increased to five times the concentration in the climatological simulation, which was designed to understand the aerosol effect under extreme pollution conditions, and does not reflect the actual observation of aerosols.

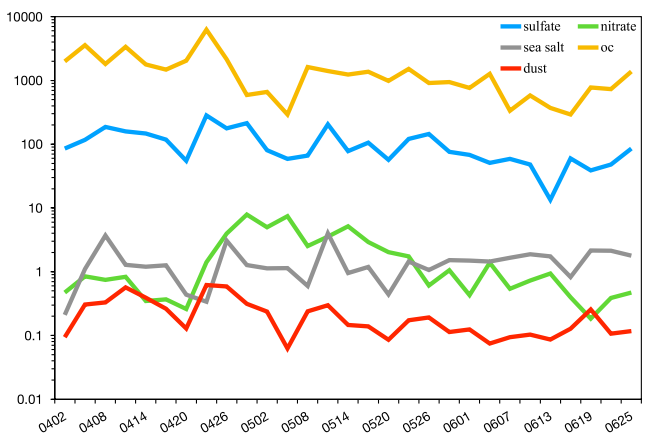

Figure 2. The number concentration (cm^{-3}) of the water-friendly aerosols: sulfate (blue), nitrate (green), sea salt (gray), organic carbon (OC) (yellow) and ice-friendly aerosols: dust (red) from 2 April 2020 to 25 June for every 3 days.

From Figure 2, we also found that OC dominates the number concentration of WF aerosols. Observation data (Bian et al., 2014) suggests the OC aerosol has a relatively large fraction of mass in the smaller condensation mode, leading to the higher number concentration in the calculation assuming aerosols are externally mixed. External mixing means all particles consist of a single chemical composition, unlike internal mixing, which implies that each particle contains all chemical components, the aerosol state is typically between the internal and external mixing states. The relatively flat size distribution of the OC is beneficial to CCN activation in that size is suggested to be more important than composition in determining CCN activity (Dusek et al., 2006; Moore et al., 2012). Additionally, even though most fresh organic species are insoluble, the aged organic species coated by soluble species such as sulfuric acid vapor are more hygroscopic and can be activated as CCN;

some observational studies have found that the carbonaceous species coupled with sulfate, nitrite, and ammonium account for a larger fraction in the condensation mode aerosols with more even size distribution (Furutani et al., 2008; Novakov & Penner, 1993). To further evaluate the potential bias in our estimation with assumed external mixing, we estimated the actual number concentration of aerosols in the condensation mode based on the measurement by a Scanning Mobility Particle Sizer (SMPS) at HKUST. We used the SMPS data that was available for April 2021 and for the diameter range of 10–763 nm, to evaluate the results of our number concentration calculations for the period spanning from April to June in 2020. Assuming the local size distribution of aerosols is time-invariant, we can establish a relation between the condensation mode number concentration and $PM_{2.5}$ mass concentration. Applying this relationship to the $PM_{2.5}$ data for April to June 2020 yields an estimation of condensation model number concentration for the period, which ranges between 231 and 4,281 cm^{-3}. This range is roughly consistent with our estimation, including all sizes and assuming external mixing, which ranges from 620 to 5,458 cm^{-3}, Therefore, while the external mixing state assumption used in our estimation is not the reality (Riemer et al., 2019), it is reasonable to use those estimation results to approximate the variability of the number concentration of WF aerosols in this study.

3. Results

3.1. Impacts on Precipitation

To better understand how aerosols affect the initiation of convection, we compared the composite radar reflectivity at 16 UTC and 17 UTC on 27 June in Figure 3. Reducing the WF aerosol leads to earlier convection triggering. Specifically, CI occurred at an early time at 16 UTC in the two simulations with minimal WF aerosol simulations: WminImin and WminImax (not shown). The earlier triggered convection cell near the island area is consistent with the observation (Figure 3a), which also shows convection near the island area, albeit with positional deviation. In other experiments, as shown in the last two rows of Figure 3, the CI was delayed and appeared at 17 UTC over the sea area. Compared with the observation at 17 UTC (Figure 3b), the simulated convection over the ocean is stronger and slightly to the east. By reducing the WF aerosol and increasing the IF aerosol in the WminImax simulation, the CI is accelerated and intensified as shown in Figure 3f. The maximum reflectivity of the convection cell in the island area is comparable to the observed value, while the convective area is smaller compared to the observation due to the delayed development. In addition, reducing the IF aerosol, the convection occurs in a relatively larger range at the early stage, as shown in Figures 3e and 3g. In the following times, which are not shown here, the development of two convection cells was all observed but with a delayed onset in all the simulations. The two convection cells further developed, moved eastward and merged afterward. We also notice that in the extremely polluted scenario, shown in Figure 3h, the convection onset is also delayed.

The accumulated precipitation in the simulations from 12 UTC, 27 June, to 06 UTC, 28 June, is shown in Figure 4. We first compare the precipitation intensity and spatial pattern for all experiments. From Figures 4a–4e, it can be found that the precipitation patterns and intensity are different by changing the aerosol concentrations. All the simulations with reduced aerosol concentrations in the four comparison experiments show more intense convection than the climatology simulation. The convection of simulations with lower aerosol concentrations is stronger than those with higher aerosol concentrations. For example, the precipitation of the WminImin (Figure 4e) is stronger than the WmaxImax (Figure 4b). In addition, reducing the WF and reducing IF aerosol, the precipitation center of the WminImin simulation is located near Hong Kong, and the strongest precipitation happened around Hong Kong Island (where the purple dot is in Figure 4f), which matches the observation very well. Thus, varying the aerosol conditions can change the CI, in this case, subtly, which has been analyzed. Furthermore, the intense convention centers of the two Wmin simulations have larger cores than those in other experiments in agreement with the composite reflectivity in Figure 3.

The maximum accumulated precipitation for all the experiments is shown in Figure 4. The four altered aerosol state simulations produce stronger precipitation maxima than the climatology simulation, which underestimates precipitation compared with the observation. Furthermore, the WminImin simulation with the minimal aerosol concentration predicted a maximum of approximately 190 mm, comparable with the observed rainfall of 188 mm. We noticed that when reducing the WF aerosols, the tendency of the maximum precipitation variation is different in the Imax and Imin groups. However, the comparison here is only based on the rainfall maximum point and misses the information over the whole precipitating area, so below, we further analyze the precipitation over the main precipitation area (red box in Figure 4).

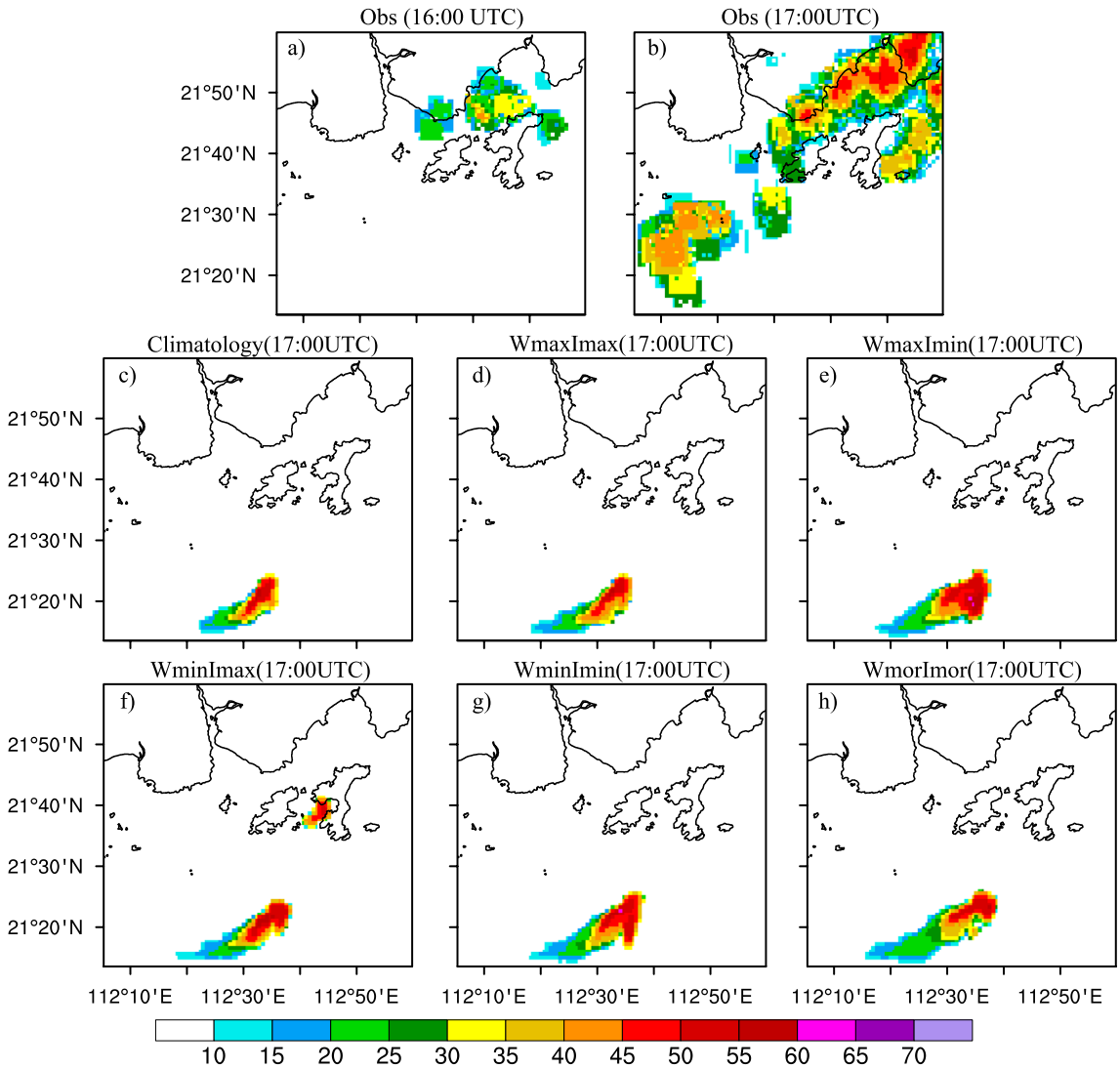

Figure 3. (a, b) Maximum composite reflectivity observation at 16 and 17 UTC, 27 June. The radar composite reflectivity for different experiments at 17 UTC, 27 June: (c) Climatology, (d) WmaxImax, (e) WmaxImin, (f) WminImax, (g) WinImin, (h) WmorImor. The small convection cells in the two Wmin simulations at 16 UTC are not shown here. The black lines indicate the coastline.

The simulation results are evaluated based on the average (Figure 5a) and maximum precipitation (Figure 5b) over the main impact area marked by the red box in Figure 4 from 18:00 UTC to 06:00 UTC. The area average (Figure 5a) and the maximum (Figure 5b) precipitation intensity in the two simulations with minimum WF aerosol (Wmin) simulations are higher than in other groups. In particular, precipitation was significantly higher at lower concentrations of WF aerosols with minimal IF aerosol concentration. The influence of varying concentrations of IF aerosols on area-averaged precipitation was inconsistent. The WmaxImin has 10% more area-averaged precipitation than the WmaxImax simulation. However, the simulations of WminImin and WminImax produced more precipitation during the early and late periods, respectively. In addition, The WminImax simulation has 30% more area-averaged precipitation than the Climatology simulation, of which the precipitation intensity is the weakest during the entire process. On the other hand, decreasing the water aerosol concentration would lead to stronger precipitation in the core area under the high IF aerosol concentration condition. The hourly precipitation maxima in the WminImin simulation are 140 mm, twice larger than that of the Climatology simulation at 22:00 UTC. Furthermore, increasing the IF aerosol with minimum WF aerosol produces more intense precipitation, and this effect is more significant in the WminImax simulation, where the precipitation intensity is higher almost over the entire precipitation process. The intense precipitation in the WmaxImax simulation also shows a weaker larger value during most precipitation times compared with the WmaxImin simulation. Figure 5c shows the

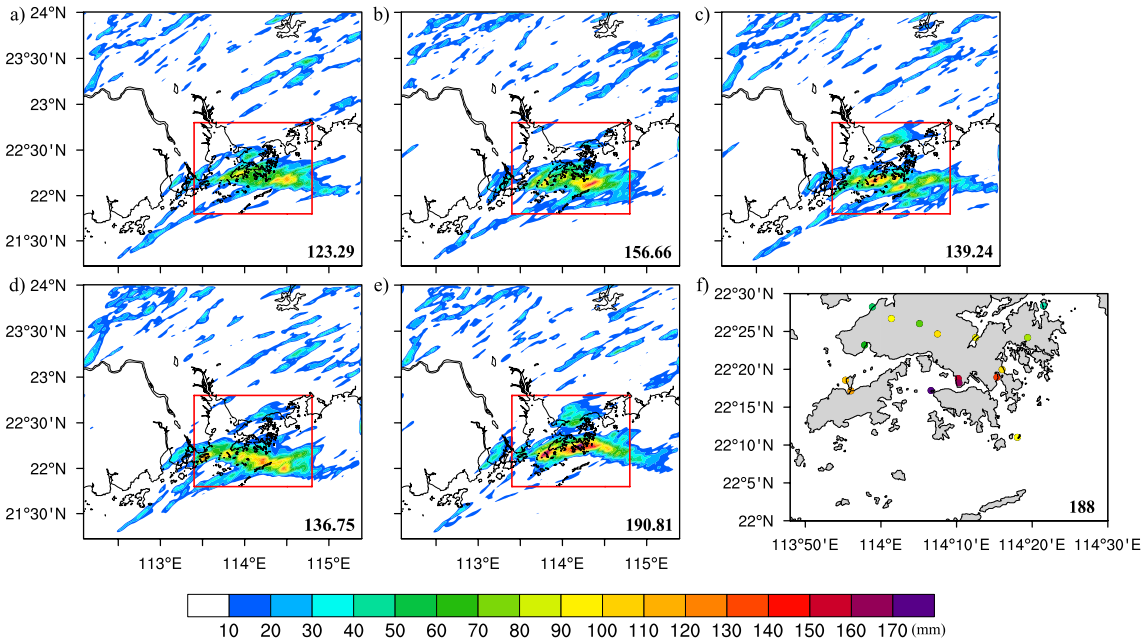

Figure 4. Accumulated precipitation from 12 UTC, 27 June to 06 UTC, 28 June of different experiments and observation: (a) Climatology, (b) WmaxImax, (c) WmaxImin, (d) WminImax, (e) WminImin, (f) observation. The red box is marked as the core precipitation area in the domain, and the numbers at the bottom right corner of each panel are the maximal grid-point accumulated precipitation (mm) of the observation and the simulations over the core area.

percentage of the area where the rainfall is larger than 20 mm in the core region. The heavy precipitation covered a larger area in the two simulations with minimum IF aerosol concentration compared with the simulations with maximum IF aerosols. Specifically, the WmaxImin has 50% larger precipitation area than the WmaxImax simulation. We can have the same conclusion for the WF aerosol impact on the precipitation area. In addition, The area covered by heavy rainfall in the WminImin simulation is almost twice as large as the Climatology run for some short periods.

Therefore, the precipitation prediction differs notably for the varying aerosol states. Changing aerosol states influenced the temporal and spatial evolution of convective systems and thereby affected the rainfall locations as well in the simulations. The WF aerosol concentration variation shows the same impact on the precipitation

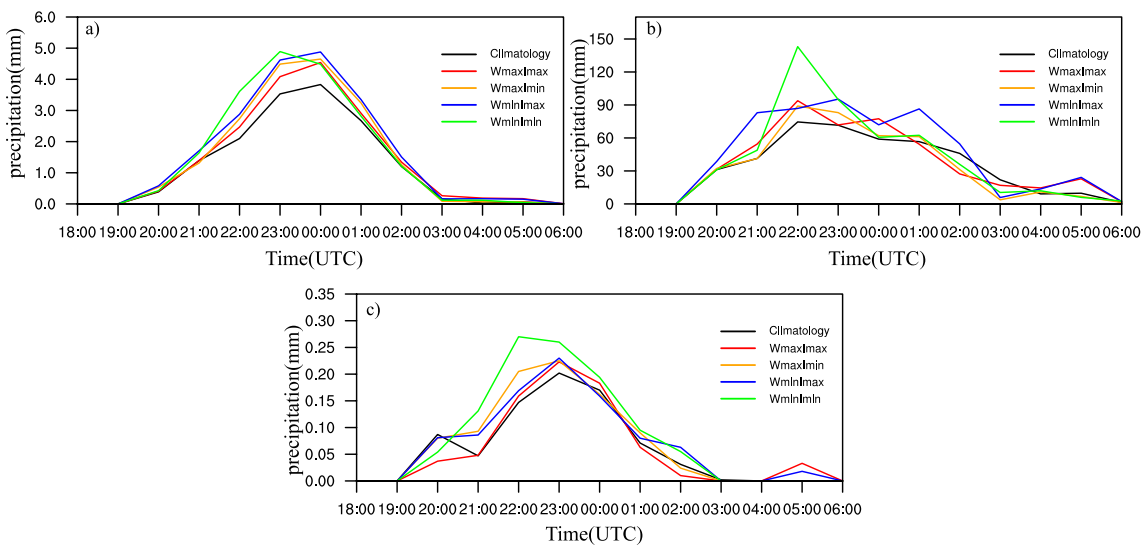

Figure 5. (a) The hourly area average precipitation of the core area (red box in Figure 4), (b) the maximum hourly precipitation in the core area, and (c) the ratio of the area with hourly rainfall larger than 20 mm to the core area.

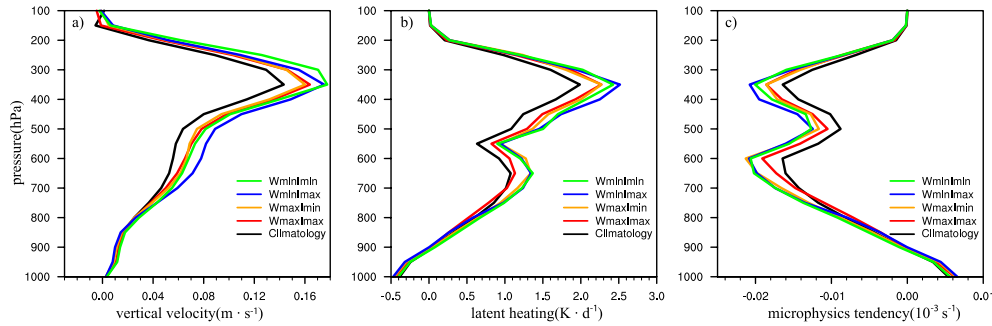

Figure 6. The vertical profiles of (a) vertical velocity ($m \cdot s^{-1}$), (b) latent heating ($K \cdot d^{-1}$) and (c) microphysics tendency for water vapor (10^{-3} s^{-1}) from 21:00 UTC to 02:00 UTC, averaged over the main precipitation area marked by the red box in Figure 4 for the five simulations.

amount and maximum precipitation intensity. Lower WF aerosol concentration expands the precipitation to a larger zone, the area-average precipitation and maximum precipitation are relatively enhanced. On the other hand, reducing the IF aerosol can lead to a larger precipitation area. The IF aerosol effect on the precipitation amount and intensity seems different. We further examined the dynamic and microphysical conditions of different aerosol states to understand the effects of the two kinds of aerosols.

3.2. Dynamic and Thermodynamic Conditions

We further examined the dynamical and microphysical conditions of different aerosol states to understand the effects of aerosols. Figure 6 shows the vertical profiles of the averaged vertical velocity from 21:00 UTC to 02:00 UTC over the core precipitation area (the red box in Figure 4). In the Wmin simulations, the latent heating, and microphysics tendency are stronger. The updraft velocity of the WminImax simulation is 60% (30%) larger than that in the Climatology simulation at 600 hPa (300 hPa). In addition, the latent heating and microphysics-induced tendency of the WminImin experiment is also higher, which is 30% and 20% more than the Climatology simulation, respectively, both at low and high-pressure levels. The impact of IF aerosols on the dynamical and microphysical conditions is different under different WF aerosol conditions. In the Wmax simulations, lowering the concentration of IF aerosols shows greater latent heat and microphysical effects, which may induce higher area-averaged precipitation in Figure 5a and larger precipitation areas in Figure 5c. On the other hand, in the two Wmin simulations, the WminImin simulation exhibits stronger ascent in the upper troposphere, the WminImax exhibits stronger ascent in the middle and lower troposphere and more latent heat release at the upper levels, which both lead to higher area-averaged precipitation compared with the Wmax simulations in Figure 5a. The difference in the profiles reveals that, in this case, the dynamical and microphysical environmental conditions are influenced by the aerosol concentration, which further affects the precipitation amount and coverage. We calculate the above variables in areas of intense precipitation next to explain the response of the convection intensity to the change in aerosol concentration.

Figure 7 presents the time-averaged vertical velocity over the $0.5° \times 0.5°$ moving box with the highest hourly precipitation in its center. Decreasing WF aerosols leads to larger vertical velocity, latent heating, and higher microphysics tendency contributing to the higher maximum precipitation in Wmin simulations (Figure 5b). The influence of the IF aerosol concentration on the precipitation intensity is distinct in the different WF aerosol concentrations. In the two Wmax simulations, slightly larger vertical velocity and more latent heating at all levels are exhibited with maximum IF aerosol concentration (WmaxImax), producing stronger maximum precipitation for almost 60% of the precipitation time in the WmaxImax simulation in Figure 5b. Additionally, the accumulative precipitation in WmaxImax is larger than WmaxImin as shown in Figure 4. In contrast, the WminImax simulation presents a significantly increased vertical velocity and latent heat release in the upper level when the IF aerosol increases, which is 40% more than in the WminImin simulation. The enhanced updraft results from the enhanced latent heating, which is probably due to the IN-induced strengthening of heterogeneous nucleation (Deng et al., 2018; Ekman et al., 2007; Min et al., 2008), then it consequently results in an increased intensity of precipitation for almost the entire precipitation life cycle in Figure 5b. These results, therefore, suggest that reducing WF aerosols or increasing IF aerosols can enhance precipitation intensity by strengthening convective

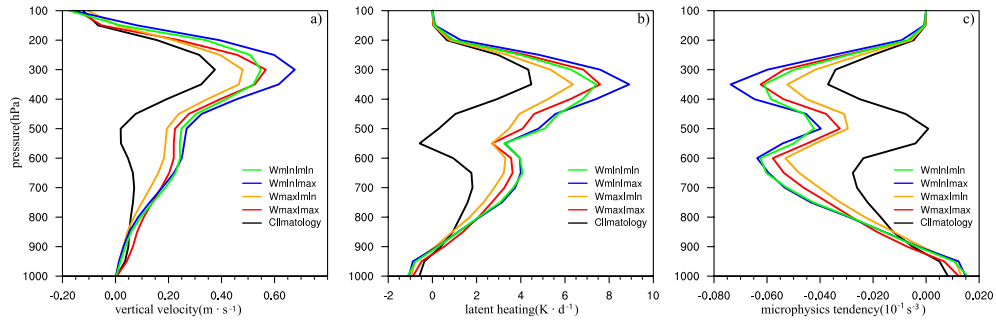

Figure 7. The vertical profiles of (a) vertical velocity ($m \cdot s^{-1}$), (b) latent heating ($K \cdot d^{-1}$) and (c) microphysics tendency for water vapor (10^{-3} s^{-1}) averaged from 21:00 UTC to 02:00 UTC over the 0.5° × 0.5° moving box with the highest hourly precipitation in its center.

motions and lead to intense precipitation. However, the effect of IF aerosols varies depending on the WF aerosol concentration, which is more significant in the reduced WF aerosol concentration condition.

We also compare the hydrometeor contents to evaluate the impact of the aerosol concentration directly. Figure 8 shows the main precipitation region mean vertical profiles of the mass mixing ratios (a-e) and vertically integrated number concentration (f) of the hydrometeors. The rainwater (Figure 8a) is directly related to the precipitation. Figure 8a shows that the area-averaged rain mass mixing ratio in the groups with reduced WF aerosol concentration is higher than the other simulations. We can see that the mass mixing ratio of liquid cloud water in Figure 8b are significantly increased in the simulations with larger aerosol concentration. The number concentration in those simulations with maximum WF aerosols is also increased, and the droplet size then would be reduced, which can expand the cloud lifetime and decrease rainwater. The graupel, snow, and ice mass mixing ratio increased significantly in the experiments with minimum IF aerosols, contributing to the precipitation increase. It appears that, first, lowering the concentration of liquid cloud droplets has an

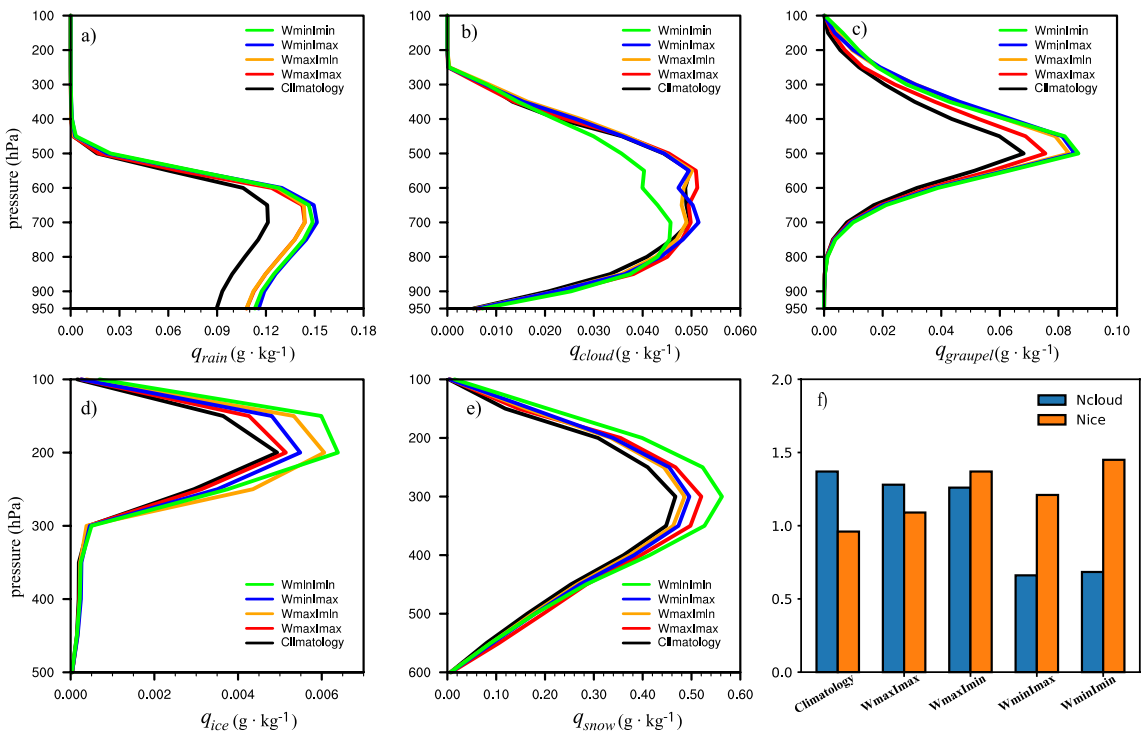

Figure 8. The vertical profiles of the mass mixing ratio (g kg^{-1}) of the (a) q_{rain}, (b) q_{cloud}, (c) $q_{graupel}$, (d) q_{ice}, (e) q_{snow} averaged from 21:00 UTC to 02:00 UTC over the core area marked as the red box in Figure 1 for the five simulations. (f) The core area mean of vertically integrated number concentration of liquid cloud (10^7 m^{-2}, blue bar), ice cloud (10^5 m^{-2}, red bar).

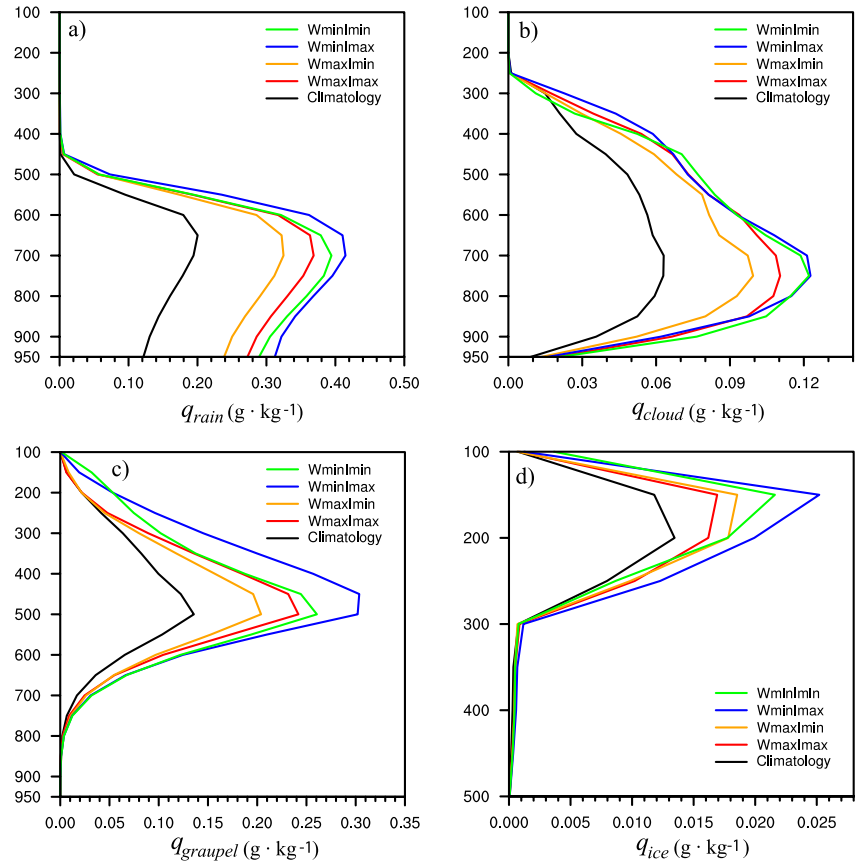

Figure 9. The vertical profiles of the mass mixing ratio (g kg^{-1}) of the (a) q_{rain}, (b) q_{cloud}, (c) $q_{graupel}$, (d) q_{ice} averaged from 21:00 UTC to 02:00 UTC over the 0.5° × 0.5° moving box as Figure 7.

important impact on convection intensity by enhancing precipitation efficiency with increased droplet size. Furthermore, the Wmin simulations have higher cloud ice number concentrations than Wmax simulations because the reduced cloud droplet concentration and larger cloud droplet size in the Wmin simulation enhance the convective strength, which in turn increases the updraft and further produces more ice in the cloud. This negative relationship between the decreased CCN and increased ice particle concentration is also found in Korolev et al. (2003) and Lance et al. (2011). Second, decreasing the concentration of IF aerosols leads to higher ice number concentrations due to the invigorated homogeneous process in the upper level, and more ice particles increase the precipitation efficiency through enhancing ice-phase precipitation growth (Kirshbaum & Smith, 2008). R. Li et al. (2017) also confirmed that pristine convective clouds tend to develop a colder (higher) top with satellite observation. Therefore, the maximum precipitation peak is found in the WminImin simulation at 22:00 UTC in Figure 5b, contributing to the higher area-averaged precipitation over the core area.

We further examined the vertical profiles of the mass mixing ratio of the hydrometer species in the moving box in Figure 9. The result shows that decreasing the concentrations of WF aerosols in the two Wmin simulations increases the mass mixing ratio of the hydrometeors, contributing to higher precipitation intensity. The two Wmin simulations produce higher cloud water, rainwater, graupel and ice particles across all the levels. In addition, increasing the IF aerosol concentration leads to higher rainwater and further enhanced convection intensity as shown in Figure 5b. Specifically, the rainwater mass mixing ratio is 10% higher in the WminImax simulation than in the WminImin simulation. This is consistent with the vertical motion enhancement due to increasing IF aerosols showed in Figure 7. The difference in rainwater between Imin and Imax conditions is even larger in the simulations with maximum WF aerosol concentrations (Wmax). On the other hand, by decreasing the WF aerosols, the mass mixing ratio of the cloud ice is increased due to the enhanced homogeneous process in the upper level, leading to the higher precipitation intensity in the WminImin simulation.

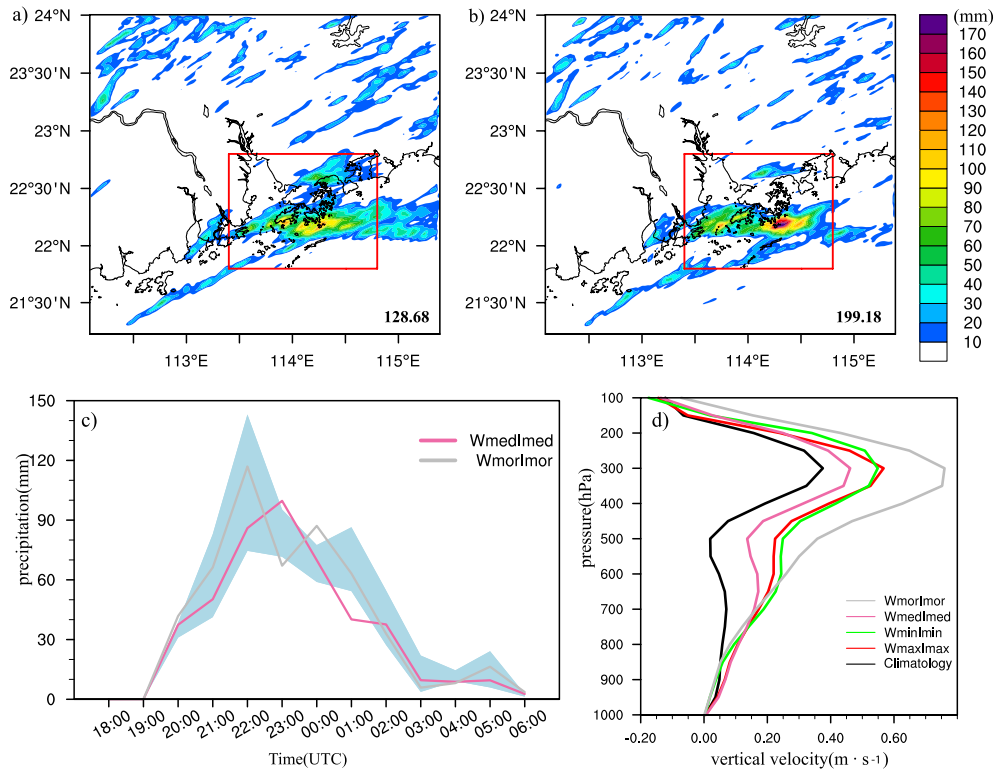

Figure 10. Accumulated precipitation from 12 UTC, 27 June to 06 UTC, 28 June: (a) WmedImed, (b) WmorImor. (c) The maximum hourly precipitation over the core area, the shading represents the variation range at each time for simulations in Figure 5. (d) The vertical profiles of vertical velocity ($m \cdot s^{-1}$) from 21:00 UTC to 02:00 UTC, averaged over the $0.5° \times 0.5°$ moving box with the highest hourly precipitation in its center. The numbers at the bottom right corner of panels (a,b) are the maximal grid-point accumulated precipitation (mm) of the simulations over the core area.

3.3. Nonlinear Relationship Between Aerosol and Precipitation

Figures 10a and 10b show the accumulative precipitation as Figure 4 of WmedImed and WmorImor, respectively. The relationship between aerosol concentration and the resulting precipitation or vertical velocity is non-linear. An increase in aerosol concentration does not necessarily enhance precipitation or increase vertical velocity (Figure 10d). When both types of aerosols were increased, the WmedImed simulation generated relatively smaller vertical velocities compared to the WminImin simulation, whereas the WmaxImax simulation exhibits vertical velocity weaker than WminImin but stronger than WmedImed. The WmorImor simulation, representing an extremely polluted scenario, produces the highest accumulative precipitation of 199.18 mm (Figure 10b), which is slightly more than WminImin's 190.81 mm, and notably stronger high-level updraft (Figure 10d). Therefore, both the WmorImor or WminImin simulations generate more-intense rainfall. They represent extremely polluted and pristine environments, respectively, and enhance precipitation with different underlying mechanisms. The result of the WmorImor simulation with higher maximal precipitation also can be found in previous studies (Niu & Li, 2012; Fan et al., 2018; Z. Li et al., 2019). Compared to the WmaxImax simulation, the clouds in the WmorImor simulation have a more compact structure and colder cloud top (not shown). Therefore, while increased aerosol might suppress the warm rain process, the unrealistically high aerosol concentration in WmorImor probably invigorated deep convection by enhancing and delaying latent heat release (Fan et al., 2018; Rosenfeld et al., 2008).

3.4. Effect of Hygroscopicity

The hygroscopicity of the aerosols is also essential to the CCN activation, which further impacts the convection evolution. These results are all based on the same default hygroscopicity parameter, 0.4, in the aerosol-aware Thompson scheme. However, the mixing state and chemical composition will change the aerosol hygroscopicity.

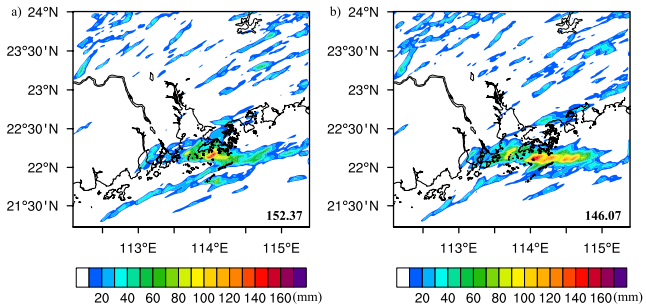

Figure 11. Accumulated precipitation from 12 UTC, 27 June to 06 UTC, 28 June: (a) WmaxImax, (b) WminImin with different hygroscopicity (0.3) from Figure 4.

Therefore, we further conducted another two simulations under maximal and minimal aerosol conditions (WmaxImax and WminImin) following Yeung et al. (2014) in which they suggested that the hygroscopicity of aerosol in Hong Kong is around 0.3. The analyzed hygroscopicity is based on the observation of the Hong Kong supersite. The precipitation simulation results are shown in Figure 11. We can see that the precipitation pattern and location are similar under different aerosol concentration conditions. However, the precipitation intensity is changed with the smaller hygroscopicity value and the precipitation simulation result is more sensitive when the aerosol concentration is minimal. Compared to the default hygroscopicity simulations, the maximal precipitation decreased by 20% for WminImin and only 5% WmaxImax.

4. Conclusion

Aerosols serving as the CCN and IN are critical factors in cloud formation. Aerosol concentration and composition variation can change the hydrometer size and number concentration, cloud evolution, and furthermore, the dynamics and thermodynamics of convection. In this study, we investigate the impact of aerosol concentration and property uncertainty on the forecast of convective rainfall in the South China coastal area with a case study. The aerosol-aware Thompson microphysics scheme was used to evaluate the aerosol effect in convection-permitting WRF simulations. We defined four aerosol concentration scenarios based on the observed variability of aerosols in Hong Kong and included another reference run using the GOCART climatology data. The simulations based on observation aerosol concentrations, lower than GOCART climatology, exhibited more precipitation and different precipitation strength. Furthermore, two additional simulations with extremely (and unrealistically) high aerosol concentration and median observation values are also conducted to examine the nonlinear relationship between aerosol concentration and precipitation intensity. In addition, we decreased the hygroscopicity from the model default to a smaller value suggested by observation and found it also increases the predicted precipitation, but the change is more notable when aerosol concentrations are low.

We used radar composite reflectivity to examine the convective initiation (CI) process in different simulations. Our findings reveal that low concentrations of WF aerosols can induce earlier CI, while simulations with relatively high levels of IF aerosols tend to produce stronger CI with two cells. In extremely polluted scenarios, convection is also delayed, even though intense precipitation occurs in the simulation. The simulation with minimum WF aerosol concentration conditions produced more and stronger convection regardless of the IF aerosol concentration, consistent with Furtado et al. (2020) who suggested that the heaviest rainfall can propagate in a clean environment. Our results also indicated that more intense precipitation is generated by reducing the WF aerosol concentration and forming larger droplet sizes under the same IF aerosol concentration situation, consistent with the results in the observatory study (Lance et al., 2011). We also found larger vertical velocity, more latent heating, and stronger microphysical tendencies at all levels in the minimal WF aerosol simulation over the intense precipitation area, contributing to the increased precipitation intensity.

The two minimal WF aerosol simulations generated comparable area-averaged precipitation, but their characteristics and mechanism are different. Increasing the IF aerosol enhances precipitation over the entire life cycle of the convective system by dynamically enhancing vertical motions, which is likely due to the increased latent heat release resulting from strengthened heterogeneous nucleation. In contrast, decreasing the IF aerosol generates more ice particles through the enhancement of homogeneous process, which leads to higher precipitation efficiency due to more efficient ice-phase precipitation growth (Kirshbaum & Smith, 2008). No significant dynamical enhancement to convection is found in this situation. As a result, a local rainfall peak with maximum intensity but a short duration is found in the simulation with the lowest concentrations of both aerosols, and it is approximately 50% higher than the prediction based on GOCART climatology. Increasing IF aerosol concentrations from WmaxImin to WmaxImax conditions has a relatively weaker dynamical effect.

Our study also demonstrated that nonlinear interaction exists between the two kinds of aerosols. In our convective system case, the effect of varying IF aerosol concentrations on precipitation intensity is amplified at reduced WF aerosol concentrations. More and stronger precipitation is generated in a clean environment, which agrees with the

previous observation and modeling studies (Furtado et al., 2020; Lebo et al., 2012). However, stronger convection is also generated in the supplementary simulation with extremely more aerosols (WmorImor). This result aligns with the deep convection invigoration theory for extremely polluted environments (e.g., Fan et al., 2013; Fan et al., 2018). However, based on our estimation with observation data, the extremely polluted situation is beyond the realistic range of aerosols variability for the South China coastal convection in the pre-summer season. In the future study, we will conduct more idealized experiments to further understand the nonlinear effects between aerosol concentration and convection intensities.

Our assessment is, admittedly, semi-quantitative, because, besides approximations used in our aerosol data analysis, the microphysics scheme also has its limitations, such as the uncertainties caused by the simplified emission treatment and assumptions in the CCN and IN process (Morrison et al., 2020; Thompson & Eidhammer, 2014). The complex interaction of two kinds of aerosols in clouds may cause microphysical perturbations that feed further into the dynamic environment, leading to changes in the cloud system. Additional complexity arises due to the dependency of aerosol effects on cloud systems and the environment, which may lead to different signs of precipitation changes in different cases when aerosol conditions are varied (Earle et al., 2011; Fan et al., 2016; Yang & Li, 2014). Therefore, more observational and simulation studies are needed to provide more accurate spatial and vertical distribution of the aerosols and further determine the co-acting and contrary effects of the two kinds of aerosols on convection. Nevertheless, our preliminary evaluation suggests that accurate aerosol measurement is essential for improving the numerical prediction of South China's pre-summer convection. Fan et al. (2016) suggested that long-term concurrent measurements of aerosol properties and meteorological fields are important for advancing our understanding and modeling capability of aerosol-cloud interaction. Such observations, if available, are beneficial not only to research efforts but also to operational weather forecasts.

Data Availability Statement

The Weather Research and Forecast model is publicly available at https://github.com/wrf-model/WRF. We archived the namelist for our simulations and ion data at (WANG, 2022).

Acknowledgments
The authors thank two anonymous reviewers for their constructive comments, which helped to improve the manuscript. We also thank Yee Ka Wong for sharing the ion observation data. We acknowledge the support of the Research Grants Council of Hong Kong SAR, China. YW and JF are supported by AoE/E-603/18, XS by HKUST 16301721. The authors thank HKUST Fok Ying Tung Research Institute and National Supercomputing Center in Guangzhou Nansha sub-center for providing high-performance computational resources.

References

Bai, L., Chen, G., Huang, Y., & Meng, Z. (2021). Convection initiation at a coastal rainfall hotspot in South China: Synoptic patterns and orographic effects. *Journal of Geophysical Research: Atmospheres*, *126*(24), e2021JD034642. https://doi.org/10.1029/2021jd034642

Bao, X., Luo, Y., & Gao, X. (2021). The synoptic impacts on the convection initiation of a warm-sector heavy rainfall event over coastal South China prior to the monsoon onset: A numerical modeling study. *Journal of Geophysical Research: Atmospheres*, *126*(14), e2020JD034335. https://doi.org/10.1029/2020jd034335

Bian, Q., Huang, X. H., & Yu, J. Z. (2014). One-year observations of size distribution characteristics of major aerosol constituents at a coastal receptor site in Hong Kong–Part 1: Inorganic ions and oxalate. *Atmospheric Chemistry and Physics*, *14*(17), 9013–9027. https://doi.org/10.5194/acp-14-9013-2014

Chang, Y.-H., Chen, W.-T., Wu, C.-M., Moseley, C., & Wu, C.-C. (2021). Tracking the influence of cloud condensation nuclei on summer diurnal precipitating systems over complex topography in Taiwan. *Atmospheric Chemistry and Physics*, *21*(22), 16709–16725. https://doi.org/10.5194/acp-21-16709-2021

Chen, G., Lan, R., Zeng, W., Pan, H., & Li, W. (2018). Diurnal variations of rainfall in surface and satellite observations at the monsoon coast (South China). *Journal of Climate*, *31*(5), 1703–1724. https://doi.org/10.1175/jcli-d-17-0373.1

Chen, Q., Yin, Y., Jiang, H., Chu, Z., Xue, L., Shi, R., et al. (2019). The roles of mineral dust as cloud condensation nuclei and ice nuclei during the evolution of a hail storm. *Journal of Geophysical Research: Atmospheres*, *124*(24), 14262–14284. https://doi.org/10.1029/2019jd031403

Colarco, P., da Silva, A., Chin, M., & Diehl, T. (2010). Online simulations of global aerosol distributions in the NASA GEOS-4 model and comparisons to satellite and ground-based aerosol optical depth. *Journal of Geophysical Research*, *115*(D14), D14207. https://doi.org/10.1029/2009jd012820

DeMott, P. J., Prenni, A. J., Liu, X., Kreidenweis, S. M., Petters, M. D., Twohy, C. H., et al. (2010). Predicting global atmospheric ice nuclei distributions and their impacts on climate. *Proceedings of the National Academy of Sciences*, *107*(25), 11217–11222. https://doi.org/10.1073/pnas.0910818107

Deng, X., Xue, H., & Meng, Z. (2018). The effect of ice nuclei on a deep convective cloud in South China. *Atmospheric Research*, *206*, 1–12. https://doi.org/10.1016/j.atmosres.2018.02.013

Du, Y., & Chen, G. (2018). Heavy rainfall associated with double low-level jets over southern China. Part I: Ensemble-based analysis. *Monthly Weather Review*, *146*(11), 3827–3844. https://doi.org/10.1175/mwr-d-18-0101.1

Du, Y., & Chen, G. (2019a). Climatology of low-level jets and their impact on rainfall over southern China during the early-summer rainy season. *Journal of Climate*, *32*(24), 8813–8833. https://doi.org/10.1175/jcli-d-19-0306.1

Du, Y., & Chen, G. (2019b). Heavy rainfall associated with double low-level jets over southern China. Part II: Convection initiation. *Monthly Weather Review*, *147*(2), 543–565. https://doi.org/10.1175/mwr-d-18-0102.1

Dusek, U., Frank, G., Hildebrandt, L., Curtius, J., Schneider, J., Walter, S., et al. (2006). Size matters more than chemistry for cloud-nucleating ability of aerosol particles. *Science*, *312*(5778), 1375–1378. https://doi.org/10.1126/science.1125261

Earle, M. E., Liu, P. S., Strapp, J. W., Zelenyuk, A., Imre, D., McFarquhar, G. M., et al. (2011). Factors influencing the microphysics and radiative properties of liquid-dominated arctic clouds: Insight from observations of aerosol and clouds during ISDAC. *Journal of Geophysical Research*, *116*(D1), D00T09. https://doi.org/10.1029/2011jd015887

Ekman, A., Engström, A., & Wang, C. (2007). The effect of aerosol composition and concentration on the development and anvil properties of a continental deep convective cloud. *Quarterly Journal of the Royal Meteorological Society*, *133*(627), 1439–1452. https://doi.org/10.1002/qj.108

Fan, J., Leung, L. R., Rosenfeld, D., Chen, Q., Li, Z., Zhang, J., & Yan, H. (2013). Microphysical effects determine macrophysical response for aerosol impacts on deep convective clouds. *Proceedings of the National Academy of Sciences*, *110*(48), E4581–E4590. https://doi.org/10.1073/pnas.1316830110

Fan, J., Rosenfeld, D., Zhang, Y., Giangrande, S. E., Li, Z., Machado, L. A., et al. (2018). Substantial convection and precipitation enhancements by ultrafine aerosol particles. *Science*, *359*(6374), 411–418. https://doi.org/10.1126/science.aan8461

Fan, J., Wang, Y., Rosenfeld, D., & Liu, X. (2016). Review of aerosol–cloud interactions: Mechanisms, significance, and challenges. *Journal of the Atmospheric Sciences*, *73*(11), 4221–4252. https://doi.org/10.1175/jas-d-16-0037.1

Furtado, K., Field, P., Luo, Y., Zhou, T., & Hill, A. (2020). The effects of cloud–aerosol interaction complexity on simulations of presummer rainfall over southern China. *Atmospheric Chemistry and Physics*, *20*(8), 5093–5110. https://doi.org/10.5194/acp-20-5093-2020

Furtado, K., Field, P. R., Luo, Y., Liu, X., Guo, Z., Zhou, T., et al. (2018). Cloud microphysical factors affecting simulations of deep convection during the presummer rainy season in southern China. *Journal of Geophysical Research: Atmospheres*, *123*(18), 10–477. https://doi.org/10.1029/2017jd028192

Furutani, H., Dall'osto, M., Roberts, G. C., & Prather, K. A. (2008). Assessment of the relative importance of atmospheric aging on CCN activity derived from field observations. *Atmospheric Environment*, *42*(13), 3130–3142. https://doi.org/10.1016/j.atmosenv.2007.09.024

Gao, X., Luo, Y., Lin, Y., & Bao, X. (2022). A source of WRF simulation error for the early-summer warm-sector heavy rainfall over South China coast: Land-sea thermal contrast in the boundary layer. *Journal of Geophysical Research: Atmospheres*, *127*(4), e2021JD035179. https://doi.org/10.1029/2021jd035179

Guo, J., Luo, Y., Yang, J., Furtado, K., & Lei, H. (2022). Effects of anthropogenic and sea salt aerosols on a heavy rainfall event during the early-summer rainy season over coastal Southern China. *Atmospheric Research*, *265*, 105923. https://doi.org/10.1016/j.atmosres.2021.105923

HKO. (2021). Hong Kong observatory. Retrieved from https://www.hko.gov.hk/en/wxinfo/pastwx/mws2021/mws202106.htm

Kirshbaum, D. J., & Smith, R. B. (2008). Temperature and moist-stability effects on midlatitude orographic precipitation. *Quarterly Journal of the Royal Meteorological Society: A Journal of the Atmospheric Sciences, Applied Meteorology and Physical Oceanography*, *134*(634), 1183–1199. https://doi.org/10.1002/qj.274

Korolev, A. V., Isaac, G. A., Cober, S. G., Strapp, J. W., & Hallett, J. (2003). Microphysical characterization of mixed-phase clouds. *Quarterly Journal of the Royal Meteorological Society: A Journal of the Atmospheric Sciences, Applied Meteorology and Physical Oceanography*, *129*(587), 39–65. https://doi.org/10.1256/qj.01.204

Lance, S., Shupe, M., Feingold, G., Brock, C., Cozic, J., Holloway, J., et al. (2011). Cloud condensation nuclei as a modulator of ice processes in arctic mixed-phase clouds. *Atmospheric Chemistry and Physics*, *11*(15), 8003–8015. https://doi.org/10.5194/acp-11-8003-2011

Lebo, Z., Morrison, H., & Seinfeld, J. (2012). Are simulated aerosol-induced effects on deep convective clouds strongly dependent on saturation adjustment? *Atmospheric Chemistry and Physics*, *12*(20), 9941–9964. https://doi.org/10.5194/acp-12-9941-2012

Li, M., Luo, Y., & Min, M. (2022). Characteristics of pre-summer daytime cloud regimes over coastal South China from the Himawari-8 satellite. *Advances in Atmospheric Sciences*, *39*(12), 1–16. https://doi.org/10.1007/s00376-021-1148-1

Li, R., Dong, X., Guo, J., Fu, Y., Zhao, C., Wang, Y., & Min, Q. (2017). The implications of dust ice nuclei effect on cloud top temperature in a complex mesoscale convective system. *Scientific Reports*, *7*(1), 1–9. https://doi.org/10.1038/s41598-017-12681-0

Li, Z., Luo, Y., Du, Y., & Chan, J. C. (2020). Statistical characteristics of pre-summer rainfall over South China and associated synoptic conditions. *Journal of the Meteorological Society of Japan. Ser. II*, *98*(1), 213–233. https://doi.org/10.2151/jmsj.2020-012

Li, Z., Wang, Y., Guo, J., Zhao, C., Cribb, M. C., Dong, X., et al. (2019). East Asian study of tropospheric aerosols and their impact on regional clouds, precipitation, and climate (EAST-AIR$_{CPC}$). *Journal of Geophysical Research: Atmospheres*, *124*(23), 13026–13054. https://doi.org/10.1029/2019jd030758

Luo, Y., Zhang, R., Wan, Q., Wang, B., Wong, W. K., Hu, Z., et al. (2017). The southern China monsoon rainfall experiment (SCMREX). *Bulletin of the American Meteorological Society*, *98*(5), 999–1013. https://doi.org/10.1175/bams-d-15-00235.1

Min, Q., Li, R., Lin, B., Joseph, E., Wang, S., Hu, Y., et al. (2008). Evidence of mineral dust altering cloud microphysics and precipitation. *Atmospheric Chemistry and Physics Discussions*, *8*, LF99–8557.

Miyamoto, Y. (2021). Effects of number concentration of cloud condensation nuclei on moist convection formation. *Journal of the Atmospheric Sciences*, *78*(10), 3401–3413. https://doi.org/10.1175/jas-d-21-0058.1

Moore, R., Cerully, K., Bahreini, R., Brock, C., Middlebrook, A., & Nenes, A. (2012). Hygroscopicity and composition of California CCN during summer 2010. *Journal of Geophysical Research*, *117*(D21). https://doi.org/10.1029/2011jd017352

Morrison, H., van Lier-Walqui, M., Fridlind, A. M., Grabowski, W. W., Harrington, J. Y., Hoose, C., et al. (2020). Confronting the challenge of modeling cloud and precipitation microphysics. *Journal of Advances in Modeling Earth Systems*, *12*(8), e2019MS001689. https://doi.org/10.1029/2019MS001689

Niu, F., & Li, Z. (2012). Systematic variations of cloud top temperature and precipitation rate with aerosols over the global tropics. *Atmospheric Chemistry and Physics*, *12*(18), 8491–8498. https://doi.org/10.5194/acp-12-8491-2012

Novakov, T., & Penner, J. (1993). Large contribution of organic aerosols to cloud-condensation-nuclei concentrations. *Nature*, *365*(6449), 823–826. https://doi.org/10.1038/365823a0

Qian, Q., Lin, Y., Luo, Y., Zhao, X., Zhao, Z., Luo, Y., & Liu, X. (2018). Sensitivity of a simulated squall line during Southern China monsoon rainfall experiment to parameterization of microphysics. *Journal of Geophysical Research: Atmospheres*, *123*(8), 4197–4220. https://doi.org/10.1002/2017jd027734

Riemer, N., Ault, A., West, M., Craig, R., & Curtis, J. (2019). Aerosol mixing state: Measurements, modeling, and impacts. *Reviews of Geophysics*, *57*(2), 187–249. https://doi.org/10.1029/2018rg000615

Rosenfeld, D., Lohmann, U., Raga, G. B., O'Dowd, C. D., Kulmala, M., Fuzzi, S., et al. (2008). Flood or drought: How do aerosols affect precipitation? *Science*, *321*(5894), 1309–1313. https://doi.org/10.1126/science.1160606

Sun, X., Luo, Y., Gao, X., Wu, M., Li, M., Huang, L., et al. (2021). On the localized extreme rainfall over the Great Bay Area in South China with complex topography and strong UHI effects. *Monthly Weather Review*, *149*(8), 2777–2801. https://doi.org/10.1175/mwr-d-21-0004.1

Thompson, G., & Eidhammer, T. (2014). A study of aerosol impacts on clouds and precipitation development in a large winter cyclone. *Journal of the Atmospheric Sciences*, *71*(10), 3636–3658. https://doi.org/10.1175/jas-d-13-0305.1

Wang, H., Luo, Y., & Jou, B. J.-D. (2014). Initiation, maintenance, and properties of convection in an extreme rainfall event during SCMREX: Observational analysis. *Journal of Geophysical Research: Atmospheres*, *119*(23), 13–206. https://doi.org/10.1002/2014jd022339

Wang, Y. (2022). Namelist and ion observation data [Dataset]. Zenodo. https://doi.org/10.5281/zenodo.7401445

Wong, Y. K., Liu, K. M., Yeung, C., Leung, K. K., & Yu, J. Z. (2022). Measurement report: Characterization and source apportionment of coarse particulate matter in Hong Kong: Insights into the constituents of unidentified mass and source origins in a coastal city in southern China. *Atmospheric Chemistry and Physics*, *22*(7), 5017–5031. https://doi.org/10.5194/acp-22-5017-2022

Wu, M., Luo, Y., Chen, F., & Wong, W. K. (2019). Observed link of extreme hourly precipitation changes to urbanization over coastal South China. *Journal of Applied Meteorology and Climatology*, *58*(8), 1799–1819. https://doi.org/10.1175/jamc-d-18-0284.1

Yang, X., & Li, Z. (2014). Increases in thunderstorm activity and relationships with air pollution in southeast China. *Journal of Geophysical Research: Atmospheres*, *119*(4), 1835–1844. https://doi.org/10.1002/2013jd021224

Yeung, M. C., Lee, B. P., Li, Y. J., & Chan, C. K. (2014). Simultaneous HTDMA and HR-ToF-AMS measurements at the HKUST Supersite in Hong Kong in 2011. *Journal of Geophysical Research: Atmospheres*, *119*(16), 9864–9883. https://doi.org/10.1002/2013jd021146

Yin, J.-F., Wang, D.-H., Liang, Z.-M., Liu, C.-J., Zhai, G.-Q., & Wang, H. (2018). Numerical study of the role of microphysical latent heating and surface heat fluxes in a severe precipitation event in the warm sector over southern China. *Asia-Pacific Journal of Atmospheric Sciences*, *54*(1), 77–90. https://doi.org/10.1007/s13143-017-0061-0

Yu, S., Luo, Y., Wu, C., & Xu, W. (2023). Subseasonal variations of convective and microphysical characteristics of extreme precipitation over the Pearl River Delta at monsoon coast. *Journal of Geophysical Research: Atmospheres*, *128*(3), e2022JD037804. https://doi.org/10.1029/2022jd037804

Yu, S., Luo, Y., Wu, C., Zheng, D., Liu, X., & Xu, W. (2022). Convective and microphysical characteristics of extreme precipitation revealed by multisource observations over the Pearl River Delta at monsoon coast. *Geophysical Research Letters*, *49*(2), e2021GL097043. https://doi.org/10.1029/2021gl097043

Zhang, S., Liang, Z., Wang, D., & Chen, G. (2022). Nocturnal convection initiation over inland South China during a record-breaking heavy rainfall event. *Monthly Weather Review*, *150*(11), 2935–2957. https://doi.org/10.1175/mwr-d-21-0264.1

Zhao, X., Lin, Y., Luo, Y., Qian, Q., Liu, X., Liu, X., & Colle, B. A. (2021). A double-moment SBU-YLIN cloud microphysics scheme and its impact on a squall line simulation. *Journal of Advances in Modeling Earth Systems*, *13*(11), e2021MS002545. https://doi.org/10.1029/2021ms002545

Zhou, A., Zhao, K., Lee, W.-C., Ding, Z., Lu, Y., & Huang, H. (2022). Evaluation and modification of microphysics schemes on the cold pool evolution for a simulated bow echo in southeast China. *Journal of Geophysical Research: Atmospheres*, *127*(2), e2021JD035262. https://doi.org/10.1029/2021jd035262